JOTCS A
Journal of the Turkish Chemical Society
Section: A
Chemistry

TURKISH CHEMICAL SOCIETY

Optimizing Experimental Parameters for Rietveld Refinement of Powder X-ray Diffraction from Small Gold Nanocrystals

Hamidreza Hekmatjou[1], Hande Öztürk[1*]

[1]Özyegin University, Department of Mechanical Engineering, İstanbul, 34794, Turkey.

Abstract: Lattice parameters, average crystal sizes and apparent microstrains obtained from Rietveld refinement of powder diffraction data from gold nanopowders of 5-30 nm size are systematically investigated. A computational workflow is introduced where atomistic models of gold nanocrystals are created, and corresponding analytical diffraction data are computed and refined. The effect of nanocrystal size, nanocrystal shape, step size of the diffraction data and refinement range on the refined parameters are separately discussed for developing an optimized Rietveld refinement strategy for accurate sample characterization. Results show that a step size no greater than 0.2° ensures stable refined lattice parameters, crystal sizes and microstrains for gold nanocrystals smaller than 30 nm. For larger nanocrystals, smaller step sizes are necessary. Accuracy of refined lattice parameters are dependent on the refinement range more strongly for smaller nanocrystals than larger ones. Depending on the shape of the nanocrystal, limited refinement range may result in over or underestimations of the lattice parameter, hence extended refinement ranges are suggested for highest accuracy. Refined crystal sizes are underestimated for ideal crystalline nanospheres while they are overestimated for ideal crystalline nanocubes. This behavior stems from the incompatible Scherrer shape constant assumed in the refinement software. Finally, microstrains refined from energy-minimized gold nanospheres are significantly overestimated for smaller nanocrystals than larger ones for limited refinement range. However, if the refinement range includes four to five high-intensity Bragg peaks, then the refined microstrains stabilize irrespective of the nanocrystal size.

Keywords: Rietveld refinement, powder X-ray diffraction, nanocrystals, crystallographic analysis.

Submitted: September 14, 2023. **Accepted:** May 3, 2024.

Cite this: Hekmatjou H, Öztürk H. Optimizing Experimental Parameters for Rietveld Refinement of Powder X-ray Diffraction from Small Gold Nanocrystals. JOTCSA. 2024;11(3): 1037-54.

DOI: https://doi.org/10.18596/jotcsa.1358713

***Corresponding author's E-mail:** hande.ozturk@ozyegin.edu.tr

1. INTRODUCTION

The relation between internal structure and material property is a key area in materials science since several properties are determined by the particular way atoms arrange themselves inside the material. Hence, developing reliable, robust and non-invasive methods to characterize internal structure of materials is critical to understand and engineer their properties. For crystalline materials, X-ray diffraction is a popular method with non-destructive, high throughput, non-invasive properties, capability to achieve structural information with sub-Ångström level resolution with a wide range of application modalities. The analytical theory behind X-ray diffraction is well established and successfully implemented in experimental analysis routines for regular crystalline materials with single crystalline or powder forms. Rietveld refinement(1), one of the most used crystallographic solution algorithms named after its developer, is a powerful method that allows for solving for the crystallographic properties of a sample from its powder diffraction (neutron or X-ray) data. This is accomplished by following three steps: **1)** Building an initial unit cell model assumed to be representative of the atomic configuration in the sample, **2)** calculating its corresponding theoretical diffraction data, and **3)** refining the theoretical data by iteratively adjusting the unit cell parameters and recalculating until it fits to the measured diffraction data with a predetermined tolerance. Once completed successfully, this iterative optimization procedure results in the crystallographic solution of the sample which contains detailed description of the crystal structure, including atomic positions, thermal vibrations of the atoms around lattice positions, the

size of the crystalline domain, etc. This crystallographic solution is not unique however, because while the structural information sought for is 3D in real space, the data that is analyzed is 1D, forbidding a one-to-one mapping of number of unknowns to number of measurements. Hence, it is not uncommon that the optimization algorithm gets stuck at a local minimum in the solution space or does not converge to a solution at all. But currently there are improved mathematical algorithms and experimental procedures which help avoid these local minima to an extent, making novel Rietveld refinement software to be more robust compared to their initial versions. Nonetheless, one must be aware of the uniqueness problem of the obtained crystallographic solution and validate it with complementary measurements techniques. This is critical especially for crystallographic analysis of multi-phase material samples, unknown crystals and nanocrystalline powders.

Nanocrystals may seem like nanoscale versions of classical crystalline materials; however, they do not satisfy some of the critical assumptions behind the theory of diffraction, which is atomic periodicity over long ranges. This brings several complications into their diffraction analysis procedures. First, diffraction peaks of nanocrystalline powders are extremely broad compared to their bulk counterparts causing significant overlap between neighboring Bragg peaks. This causes peak finding and peak fitting algorithms to fail to correctly identify all peaks. Since the number of atomic planes in a nanocrystal diffracting at a particular Bragg angle is much less than that of a regular crystal, complete destructive interference between Bragg angles is impossible(2) leading to a significant amount of diffuse scattering between Bragg angles(3). This makes background removal during data analysis challenging. Finally, the intensities of Bragg peaks measured from nanocrystalline powders of small particles are relatively weak and may easily be lost under the background signal causing misidentification of the phase of the powder.

In addition to the numerical challenges of analyzing diffraction patterns of nanocrystalline powders, an accurate formulation to relate the diffraction intensity distribution to structural parameters of nanocrystals is also lacking. This is a problem for step 2 of the Rietveld refinement algorithm: The cif files of nanocrystals are particle size dependent and are not available in databases. Hence, the initial information about the atomic stacking of the analyzed nano-powder is accessed from the cif files of bulk counterparts which do not necessarily reflect the nano-characteristic features of the sample and cause incompatibility between the theoretical and the actual measured diffraction signal. This incompatibility leads to the resulting Rietveld refinement to be biased, leading to incorrect characterization of the studied sample. Our past work confirmed such inaccuracies in the refinement of small nanocrystalline powders: for example, we found that due to the extreme peak broadening phenomenon, the scattering probability of an irradiated monodispersed particle ensemble was not correctly predicted by the classical Klug and Alexander formulation(4) suggesting that the multiplicity of reflection for small nanocrystals was different than their bulk counterparts. This caused the one-to-one relation between the particle and intensity statistics to break down for nanocrystals smaller than 30 nm or so(5). Similar conclusions were drawn by other researchers as well(6). We observed that even when the nanocrystal was modeled identical to a bulk crystal with nanometric dimensions, its analytical diffraction data resulted in inaccurate lattice parameters from Rietveld analysis(7). These inaccuracies decayed with increasing crystal size confirming that the small sizes of nanocrystals were to blame for the large deviations in peak intensity positions from analytically obtained Bragg angles.

These examples point to the great care to be exercised while interpreting diffraction analysis results of nanocrystalline powders performed by algorithms based on classical diffraction theory. Moreover, they motivate systematic investigations to evaluate the performance of Rietveld refinement on the diffraction data of nanocrystalline powders since powder diffraction is still the first method to confirm appropriate synthesis of such materials. Ultimately these efforts would lead to a set of best practices for performing diffraction experiments and analyzing measurements appropriately for reliable structural analysis of nanocrystalline powders with quantified errors. With this goal, here we investigated how the results of Rietveld refinement performed on powder diffraction data from gold nanocrystalline particles vary with the step size of collected diffraction data and refinement range selected in Rietveld analysis. To alleviate ambiguities such as noise and statistical uncertainties which may prevent us from drawing clear conclusions, we performed our investigation on computer simulated diffraction data. Ideal crystalline, spherical and cubic gold nanocrystals and energy-minimized spherical gold nanocrystals at 0 K were used as the diffracting samples since these models were structurally simple and served to isolate sources of sample-specific error and accurately quantify them in the Rietveld analysis. Particle size was limited from 5 to 30 nm because the 5 nm crystal size was small enough to enhance nano-specific features in the diffraction data and 30 nm size was large enough to observe bulk-size features in the diffraction data. Finally, using these models, three crystallographic parameters namely, lattice parameters, average crystal sizes and average microstrains obtained from Rietveld refinement were systematically analyzed.

2. FUNDAMENTAL FORMULATION OF RIETVELD REFINEMENT

The theoretical basis of Rietveld refinement lies in the calculation of expected diffraction pattern from an investigated sample based on combining **a)** sample related parameters such as the assumed crystal structure model with **b)** instrumental parameters of the experimental setup used to

measure diffraction data such as the wavelength of X-rays, the profile of the incoming beam, polarization of the X-rays, etc. Then this theoretical pattern is refined against measured diffraction data until a predetermined extent of agreement is achieved.

The assumed crystal structure is built from the cif (crystallographic information file) file of the sample which contains average crystallographic information about the unit cell such as its dimensions and shape, the relative positions (u,v,w) and types of atoms in the cell, their thermal vibration parameters etc. To associate the diffracting sample with its expected diffracted intensity distribution, one must start from this unit cell. Hence, the expected scattering amplitude from a single unit cell oriented at a given hkl Bragg condition is formulated as the total scattering amplitude of its constituent atoms and called the structure factor F_{hkl}. For a monatomic unit cell consisting of a single atom type, F_{hkl} is given as(8):

$$F_{hkl} = \sum_{j=1}^{N_c} f_j \, exp\left(2\pi i \left[hu_j + kv_j + lw_j\right]\right) \qquad \text{(Eq.1)}$$

Here N_c is the number of atoms in the unit cell, f is the atomic scattering amplitude for a single atom that depends on the energy of X-rays and the scattering direction, and $[u_j, v_j, w_j]$ is the fractional coordinate of atom j with respect to the unit cell dimensions along x, y and z axes. The diffraction intensity, which is the measurable quantity, is proportional to the squared magnitude of F_{hkl}. To obtain the full diffraction pattern, we multiply the intensity formula of the unit cell with terms taking care of diffraction probability of an irradiated crystal as well as instrumental parameters. The effect of instrumental parameters on the expected diffraction profile is formulated by convolving the sample profile by the instrument profile. Hence, an empirical form of Bragg intensity distribution can be written as[1]:

$$I_{hkl}(2\theta) \propto I_0 |F_{hkl}|^2 m_{hkl} \, T(2\theta) \, LP(2\theta) \, A(2\theta)$$
(Eq.2)

In Eq.2, I_0 is the incoming X-ray intensity which corresponds to a normalized form of the incoming photon count on the sample, m_{hkl} is the multiplicity of the hkl reflection which is the number of equivalent planes with the same interplanar distance characteristic of the unit cell, T(2θ) is the temperature factor also known as the Debye-Waller factor that models the temperature-dependent decay in the diffraction intensity resulting from dynamic motion of atoms inside the crystal, A(2θ) is the absorption factor modeling the decay in the diffraction intensity as a result of incoming photon absorption within the crystal as the X-rays travel inside and finally LP(2θ) is the Lorentz-polarization factor. LP takes care of the geometry-dependent diffraction probability variation from one Bragg peak to another and the polarization of the incoming X-ray beam. As seen, Eq.2 can easily generate the first estimate of the diffraction intensity distribution if initial crystal properties and the instrumental parameters including X-ray wavelength are provided about the investigated sample: first the Bragg angles are computed based on the Bragg's law, $2d_{hkl}sin\theta_{hkl} = \lambda$, using the type and lattice parameter of the sample's unit cell and the wavelength of the X-rays, next an analytical peak function which isusually a Gaussian, or a Lorentzian or a bifunctional combination of thoseis centered at each Bragg angle within the measurement space and each one of the peaks is assigned a maximum value computed by Eq.2, finally these peak profiles are convoluted by the instrument profile function. The later steps involve using a least square error minimization algorithm to minimize the discrepancy between this calculated intensity profile I_{calc} and measured or observed profile I_{obs} iteratively by adjusting/refining the model parameters resulting in a new estimate of I_{calc}. The minimized function takes the following form(9):

$$R_{wp} = \left\{\sum_i w_i [I_{(obs)i} - I_{(calc)i}]^2 / \sum_i w_i [I_{(obs)i}]^2\right\}^{1/2}$$
(Eq.3)

where R_{wp} is the weighted residual, I_{obs} is the observed or measured diffraction data which is analyzed, i is the dummy index referring to the angular step and w_i is the weighting factor at step i. The weighting factor is typically determined by considering the uncertainties associated with the experimental data, such as counting statistics and instrument-related factors(10, 11).

3. METHODOLOGY

In this section, the steps followed for simulation of the nanocrystal powders as well as their corresponding diffraction data and the Rietveld refinement strategy are explained.

3.1. Simulation of Nanocrystalline Powders

We studied three sets of monodispersed and ideally random powder ensembles: one consisting of ideal crystalline nanospheres, one of ideal crystalline nanocubes and one of non-ideal nanospheres resulting from minimum-energy atomic configurations obtained from Molecular Dynamics simulations at 0 K. While the first two nanocrystal models were used to obtain the performance and sensitivity of Rietveld analysis with minimized uncertainties in the investigated sample and refinable parameters, the third model was used to study the capability and robustness of Rietveld refinement to capture particle-wide fluctuations in the atomic stacking on the corresponding diffraction data. For both the spherical and cubic ideal nanocrystals, particle dimensions were set to 5, 10, 15, 20, and 30 nm. These ideal crystalline particles had their atoms situated at repeating FCC unit cells having a lattice parameter of 4.0626 Å belonging to gold at 0 K. The energy-minimized spherical nanoparticles were obtained by equilibration of ideal crystalline spherical nanoparticles at 0 K and these experienced static atomic displacements due to surface relaxation/reconstruction(12) compared

[1] These functions differ in the way they model the angular dependence of particle size and microstrain related broadening in the observed Bragg profiles.

with ideal crystalline nanospheres. Further detail on the energy minimization step is provided in our previous works(13, 14). Once the atomistic models of all nanocrystals were built, lattice parameters and particle dimensions were evaluated following the methodology described in a previous work(12). Particle sizes were calculated by considering undercoordinated surface atoms having a coordination number smaller than 12. These atoms each had a pairing atom located in opposite direction such that the line connecting them passed through the particle center and was considered one diameter line. Average particle size was obtained from the mean of all diameter lines connecting paired surface atoms. Next, the average lattice parameters were calculated by decomposing an ideal crystalline particle into repeating unit cells where each unit cell was built by one origin atom and three corner atoms positioned at <110> directions. These 4-atom groups were mapped in the corresponding equilibrated particle to calculate the lattice parameter of the energy-minimized nanospheres. For ideal crystalline spherical and cubic nanoparticles, the lattice parameters were constant within the particle. However, for the energy-minimized spherical nanocrystal, the lattice parameter varied from particle core to particle surface due to the surface relaxation/reconstruction. The crystallographic parameters of the created nanocrystal models are reported in Table 1.

Table 1: Nominal size, average size (D_{RS}, t_{RS}) and lattice parameters (a_{RS}) and total number of atoms of the nanocrystal models from real space (RS) calculations. Uncertainties reported are standard deviations from the mean.

Size	Spherical particles					Cubic particles		
	# of atoms	Ideal Crystalline		Energy minimized		# of atoms	Ideal Crystalline	
		D_{RS} (nm)	a_{RS} (Å)	D_{RS} (nm)	a_{RS} (Å)		t_{RS} (nm)	a_{RS} (Å)
5	3589	4.606±0.155	4.0626	4.589±0.138	4.0499±0.03446	7814	4.875	4.0626
10	28897	9.486±0.149	4.0626	9.470±0.132	4.0567±0.0242	66327	10.156	4.0626
15	106114	14.773±0.152	4.0626	14.760±0.1351	4.0594±0.0191	210939	15.032	4.0626
20	231477	19.235±0.152	4.0626	19.224±0.1358	4.0608±0.0158	485151	19.907	4.0626
30	781145	28.981±0.153	4.0626	28.973±0.137	4.0617±0.0118	1721477	30.470	4.0626

3.2. Computation of Diffraction Datasets

Analytical powder diffraction data was computed by the Debye scattering equation(15). This equation is derived by formulating the expected diffraction intensity from a single particle, and then integrating the diffracted intensity distribution over the surface of a unit sphere(16) in reciprocal space. This last step results in the orientational average of the expected diffraction signal from the particle, which corresponds to the normalized intensity distribution from a monodispersed particle ensemble (powder) with infinitely many identical particles of independent orientations. The Debye equation takes the following form:

$$\langle I(2\theta)\rangle = \sum_{n=1}^{N}\sum_{m=1}^{N} f_n f_m \frac{sin(qr_{nm})}{qr_{nm}} \qquad \text{(Eq.4)}$$

Here N is the number of atoms in a single particle making up the powder, q is the magnitude of the momentum transfer vector given as $q = |\vec{q}| = \frac{4\pi sin\theta}{\lambda}$ where θ is half the scattering angle and $r_{nm} = |\vec{r}_n - \vec{r}_m|$ is the magnitude of the interatomic distance vector connecting the n'th and m'th atoms. As seen, the Debye scattering equation is a general formulation of average diffraction intensity from a group of atoms, irrespective of whether the particle is crystalline or amorphous. Secondly, the orientational average of the intensity distribution is computed analytically, therefore the resulting intensities are free of statistical uncertainties from finite scattering probability of the irradiated crystals(4, 17) or uncertainty due to the photon counting processes. Hence, we selected this formulation and evaluated Eq.4 for our nanocrystalline powder models to obtain our diffraction datasets. However, instead of directly evaluating Eq.4, we used the optimized Debyer(18) algorithm to compute the diffraction data to reduce the computation time. An X-ray wavelength of 1 Å was selected and the diffraction data was computed over an angular range of [5°-180°] for all nanocrystal models. To investigate the effect of step size of the diffraction data on the refined parameters, all datasets were computed with 4 different step sizes: 0.01°, 0.05°, 0.1° and 0.2°. Figure 1 demonstrates the computed intensities from ideal crystalline spherical, ideal crystalline cubic and energy-minimized spherical nanocrystals of 5 nm nominal size.

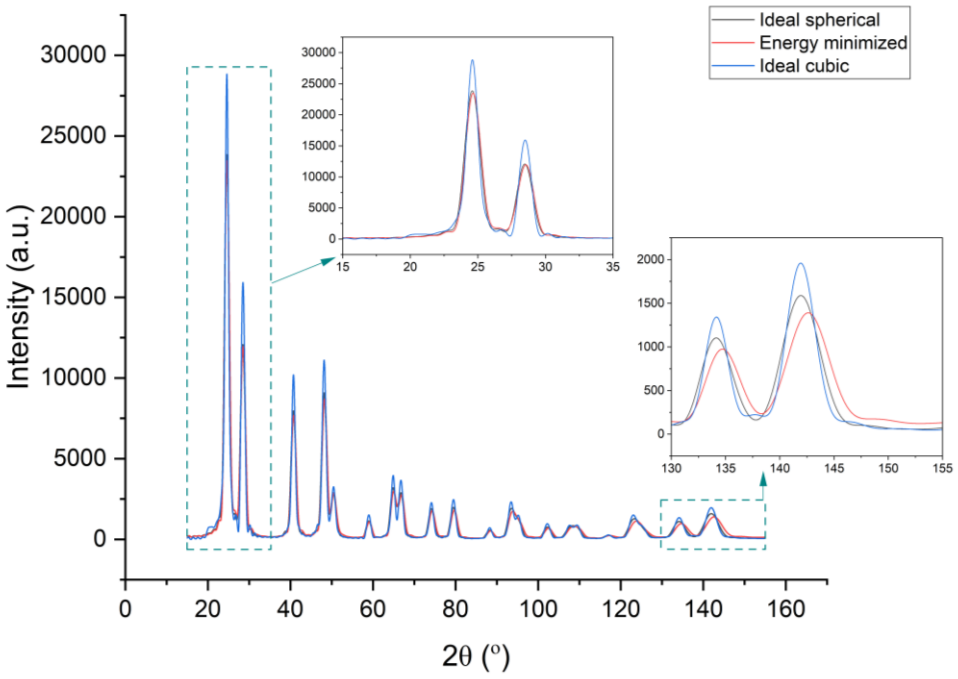

Figure 1: The computed powder diffraction profiles of the studied nanocrystal powders (λ = 1 Å). The differences between the computed profiles are enhanced at higher diffraction angles.

3.3. Rietveld Refinement of the Diffraction Data

We used the open source software GSAS II(19) to perform Rietveld refinement on our diffraction data. Before each refinement, we uploaded the computed diffraction data as well as the cif file of gold, which included the unit cell properties of bulk crystalline gold tabulated in standard databases. Next, an instrument file which had hypothetical parameters corresponding to an ideal diffractometer assumed in our diffraction calculations was provided. Using the instrument and sample related parameters, a diffraction pattern was modeled by GSAS II using Eq.2 and this pattern was modified at each refinement cycle until it matched with the observed (computed) diffraction data. At the end of the refinement, three crystallographic properties were extracted: average lattice parameter was obtained from the peak centers while average crystal size and apparent microstrain (if present) were computed from peak broadening. For crystal size and microstrain calculations, Williamson-Hall method(20) was used such that the total broadening of a given Bragg peak was modeled as a combination of broadening associated with limited crystal size and local variation of the lattice parameter within the individual crystal. In this case, size-related peak broadening was modeled by the Scherrer equation(21) and microstrain was assumed to be isotropic and was allowed to vary smoothly over the diffraction angles with a tan θ dependence(22) where θ was half the scattering angle.

Table 2: Initial parameters in Rietveld refinement. Parameters indicated by an asterisk (*) are refined and those without are fixed at their initial values.

Size	Spherical particles										Cubic particles				
	Ideal Crystalline					Energy minimized					Ideal Crystalline				
	D_R* (μm)	a_R* (Å)	με	MSD (Å²)	LGmix*	D_R* (μm)	a_R* (Å)	μ*	MSD (Å²)	LGmix*	D_R* (μm)	a_R* (Å)	με	MSD (Å²)	LGmix*
5	0.00	4.0782	0	0	1.0	0.00	4.0782	100	0	1.0	0.00	4.0782	0	0	1.0
10	0.01	4.0782	0	0	1.0	0.01	4.0782	100	0	1.0	0.01	4.0782	0	0	1.0
15	0.01	4.0782	0	0	1.0	0.01	4.0782	100	0	1.0	0.01	4.0782	0	0	1.0
20	0.02	4.0782	0	0	1.0	0.02	4.0782	100	0	1.0	0.02	4.0782	0	0	1.0
30	0.03	4.0782	0	0	1.0	0.03	4.0782	100	0	1.0	0.03	4.0782	0	0	1.0

Depending on the type of the sample, different refinement strategies were followed: for ideal crystalline gold nanocrystals, lattice parameter, profile shape factor (LGmix, mixing parameter of Gaussian and Lorentzian peak profile functions), average crystal size and an arbitrary scale factor was initialized and refined. For energy-minimized gold nanospheres, microstrain was added to the refinement parameters to account for surface atom displacements resulting from energy minimization. Since the refined data were free of instrumental errors or statistical uncertainties, we did not subtract any background scattering before the refinement. This refinement scheme was consistent

with previous literature(7). Table 2 summarizes the initial values of the refinement parameters used for each nanocrystal model where D_R, a_R, με, MSD, and LGmix represent initial particle size, lattice parameter, microstrain, mean-square atom displacement, and Lorentzian-Gaussian mixing parameter, respectively. Moreover, the refined parameters are indicated by * in Table 2 whereas parameters without * were fixed at their initial values during the refinement.

Following each successful refinement, the updated values of the refined parameters were collected and systematically analyzed. Figure 2 shows how a successful refined model looks like for a 5 nm spherical (left) and cubic (right) nanocrystal. In this figure, observed intensities are the analytically computed intensities, whereas calculated intensities are the best fitted Rietveld models. The difference between the two intensities shown in turquoise color is called the residual. The lack of large variations in the residuals indicates that the fit is successful. Additionally, the blue ticks are well aligned with the centers of the computed and fitted diffraction peaks indicating that the crystal unit cell of the nanoparticles is correctly represented by the refined cif file of bulk gold.

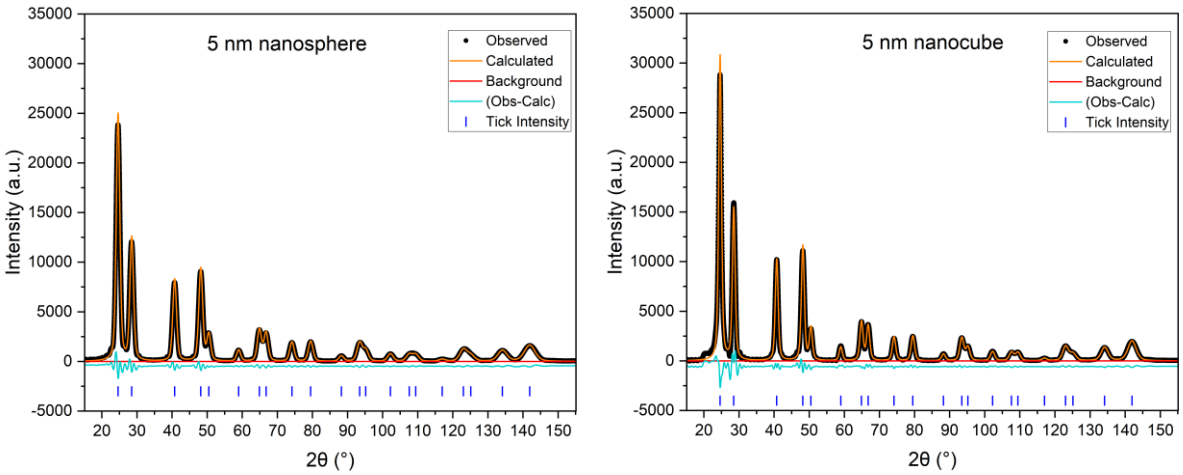

Figure 2: A successful Rietveld refinement of the diffraction data from a 5 nm ideal crystalline nanosphere (left) and a 5 nm ideal crystalline nanocube. Calculated refers to the diffraction data modeled by GSAS II, whereas Observed refers to the analytical diffraction data computed by the Debye equation. The blue tick marks show the expected positions of the Bragg peaks predicted by Bragg's law.

4. RESULTS

In this section, we investigate the variation of the refined lattice parameters, crystallite sizes and microstrains with respect to the step size of the investigated diffraction data, angular range of refinement, nanocrystal size and shape.

4.1. Accuracy of Refined Lattice Parameters

The figure 3 shows the effect of refinement range and step size of the diffraction data on the refined lattice parameters for powders consisting of ideal crystalline gold nanospheres with different diameters. In each subplot, 4 different Rietveld analysis results are seen, where the diffraction data in each was computed with a different angular step size (dθ) ranging from 0.01° to 0.2°. The purple horizontal lines in the subplots show the true lattice parameter of the gold nanocrystals which was equal to 4.0626 Å. The horizontal axis indicates the refinement range selected. As seen, the refinement range is not evenly distributed along the horizontal axis, but rather it was extended gradually by adding each new Bragg peak one by one except when there were overlapping peaks in the diffraction profile. Overlapping peaks were added to the refinement range together for better fitting quality.

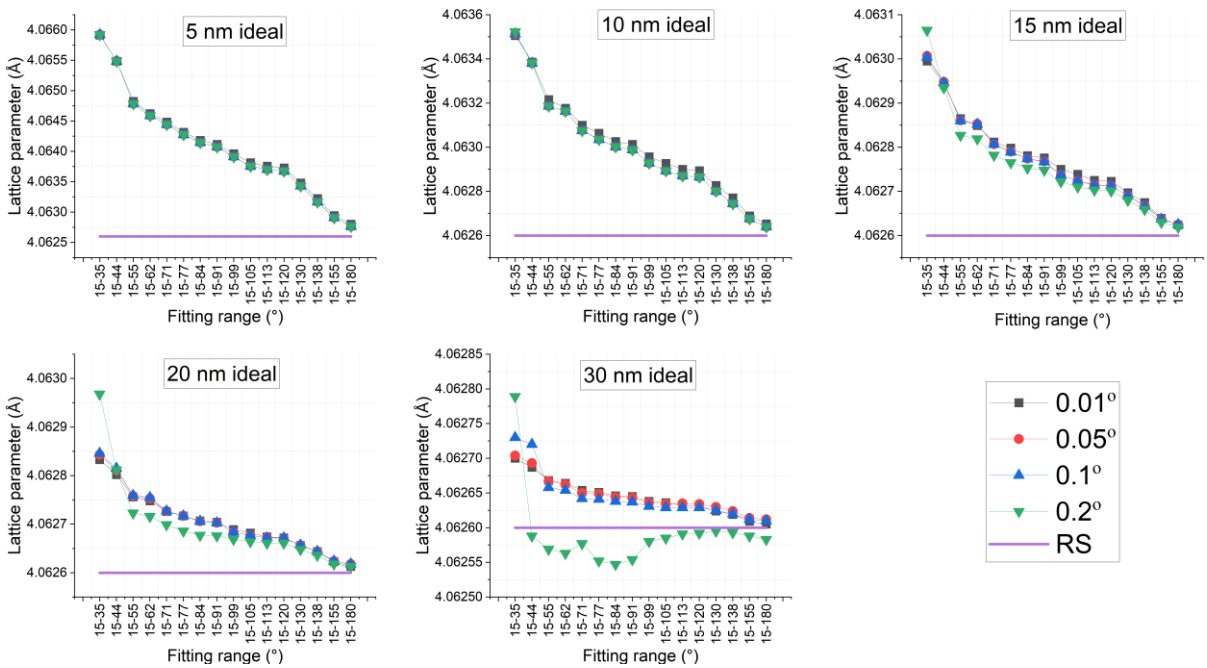

Figure 3: The variations of Rietveld-refined lattice parameter using different angular ranges for ideal crystalline gold nanospheres. RS stands for real-space calculations.

Multiple conclusions can be drawn from the figure: first, for all nanocrystal sizes, increasing the refinement range causes the extracted lattice parameters to decrease and converge to their true values. This is expected since with increasing the fitting range, we included more Bragg peaks in the Rietveld analysis which contributed to the accuracy of refined average lattice parameters(23). This trend seems to repeat for all step sizes selected in the diffraction data except for the case with dθ = 0.2°. Here significant fluctuations in the refined lattice parameter are visible especially for the largest nanocrystal, i.e., 30 nm. This can be explained on the basis of the crystal size and peak broadening relationship in the diffraction data: as formulated by Scherrer(21), an inverse relationship exists between the Bragg peak breadth and the crystal size of the diffracting object. This means that the sharpest Bragg peaks belong to the largest nanocrystal. Hence, when dθ was set to a relatively large value such as 0.2°, the peak profile was effectively sampled with too few points and the probability of missing the exact peak center increased. This directly translated to increased fluctuations in the refined lattice parameters. Secondly, in all nanocrystals, limiting the refinement range to lower angle Bragg peaks seems to cause significant overestimations in the extracted lattice parameters. Similar observations were made in a past study(7) for the same gold nanocrystal system where lattice parameters from lower-angle Bragg peaks were overestimated and higher-angle ones were underestimated, and it was mentioned that the root cause for lower-angle Bragg peaks to overestimate the true lattice parameter was the limited number of atoms in the diffracting crystallite. Here we confirm this observation as well as its particle size variation since with increasing nanocrystal size, the amount of overestimation in the refined lattice parameter for a particular refinement range decrease. The only exception is the case with dθ=0.2° for 30 nm nanocrystals where lower angle Bragg peaks first overestimated and then underestimated the true lattice parameters. Not surprisingly, this particle size also happened to result in the lowest quality of fit from Rietveld refinement when dθ=0.2° as seen in Figure 4. Here wR is the weighted residual reported by GSAS II and normalization is performed with respect to the length of the diffraction data. For 30 nm nanocrystals, the reported weighted residual was ~13%, higher than that of smaller nanocrystals with the same step size which may explain the unexpected underestimations of the lattice parameters. In fact, the normalized weighted residual plots in Figure 4 confirm the degrading quality of fit with increasing step size for all nanospheres. This shows that, the value of angular step size while collecting diffraction data is more critical for larger nanocrystals than smaller ones.

Repeating the above analysis on the diffraction data from energy-minimized spherical gold nanocrystals yields some common and some slightly different results which are summarized in Figure 5. Note that here the real-space-computed lattice parameters (RS) vary with the size of the nanocrystals and they increase with increasing size as shown in Table 1 and our previous work(7). This size dependence of lattice parameters of nanospheres is a consequence of surface reconstruction which causes the atoms in the surface region of the nanocrystals to be displaced radially inward due to the energy-minimization process resulting in smaller lattice parameters within the surface layer. However, this phenomenon is less appreciable for larger nanocrystals with smaller surface to volume ratio leading to larger average lattice parameters. Looking at the refined lattice parameters we see that they are again overestimated especially for lower angle Bragg peaks but converge to their true average values with increasing fitting range. Unlike

ideal crystalline nanospheres, here the refined lattice parameters are never underestimated even for the largest nanocrystal with the highest step size in the diffraction data. Between ideal crystalline and energy-minimized nanospheres, the former shows much smaller deviations of refined lattice parameters from the true value than the latter: for the 5 nm energy-minimized gold nanosphere with dθ=0.01°, Rietveld-refined lattice parameters are overestimated by ≈0.004 Å at most, which decay to ≈0.001 Å over the widest refinement range. The corresponding values for the ideal crystalline nanosphere are less than 0.0005 Å over all refinement ranges. These deviations decrease with increasing nanocrystal size for both particle systems. Finally, the value of the step size has negligible effect on the refined lattice parameters for all particles except for 20 and 30 nm nanocrystals.

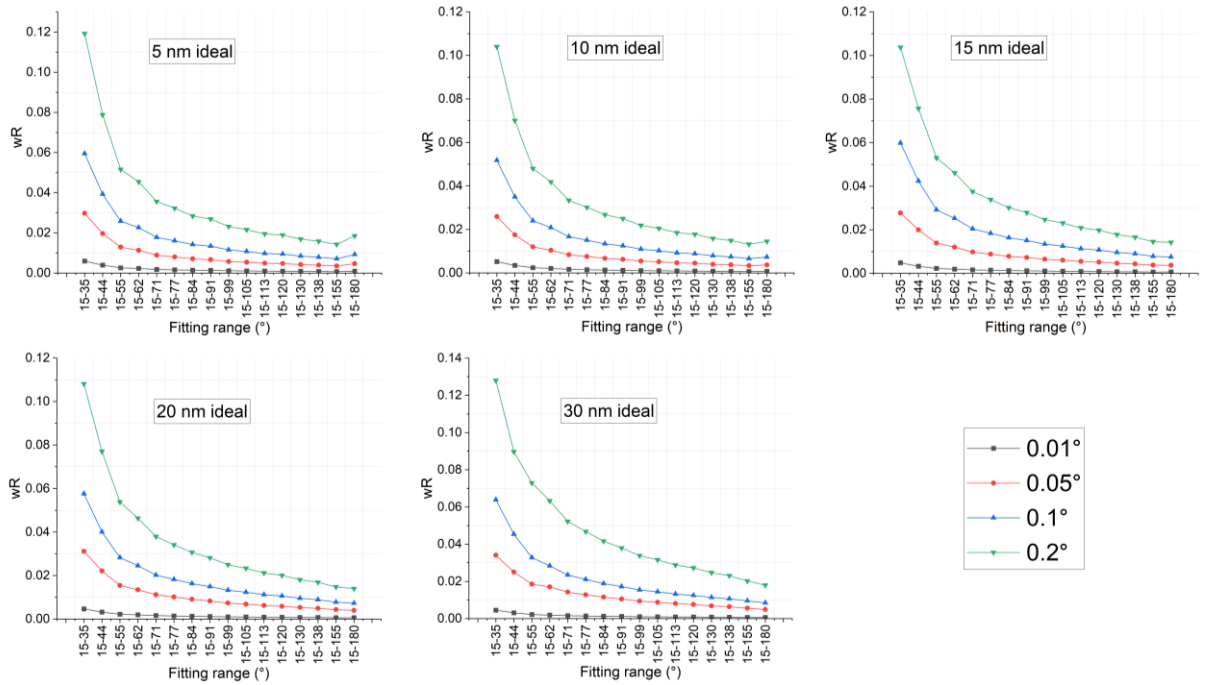

Figure 4: The weighted residuals (wR) normalized by the number of measurement points from Rietveld refinement of diffraction data computed with different step sizes of ideal crystalline gold nanospheres.

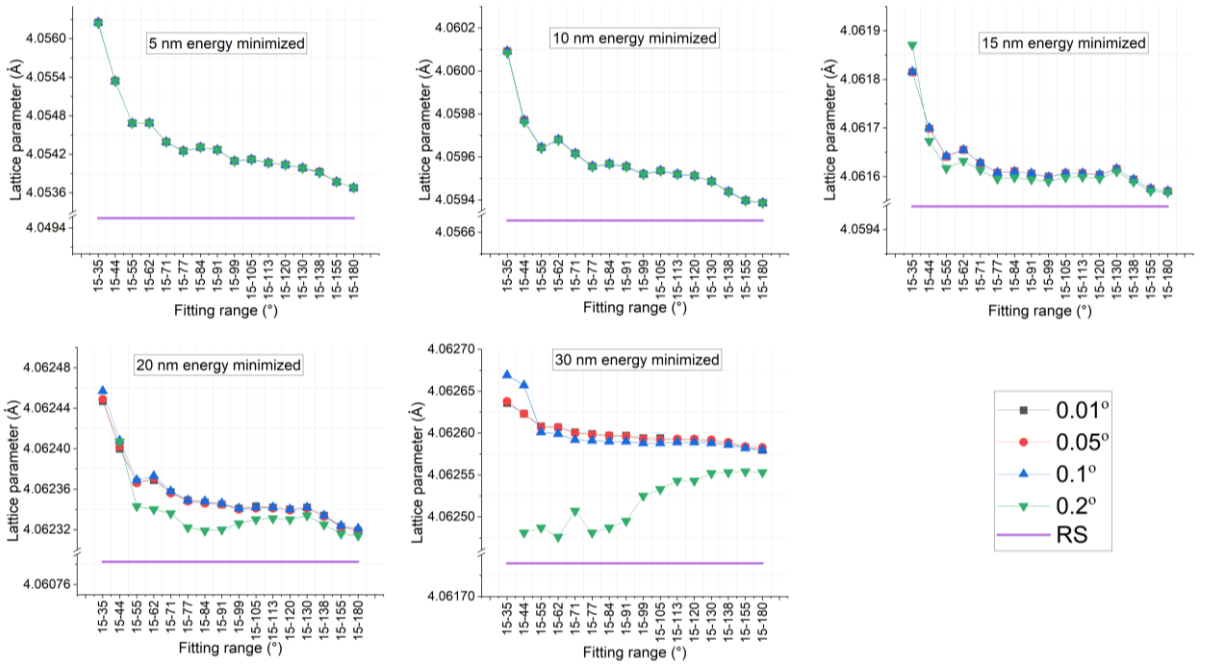

Figure 5: The variations of Rietveld refined lattice parameters using different angular ranges for energy-minimized gold nanospheres. Axis breaks on the vertical axis were used to enhance the readability of the figure.

To investigate whether the shape of the nanocrystals affects the accuracy of the Rietveld-refined lattice parameters, we repeated our analysis on the diffraction data from ideal crystalline gold nanocubes as well. Figure 6 summarizes our findings. First, we observe that except for the 5 nm nanocrystal, all other nanocubes show similar features as their spherical counterparts: 1) the refined lattice parameters approach their true values with increasing fitting range, 2) the selection of the angular step size has almost negligible effect for the smaller nanocrystals, but it causes some fluctuations in the lattice parameters of the larger nanocrystals. This can be explained by the significant peak broadening associated with the profiles of smaller nanocrystals. Unlike nanospheres, however, the refined lattice parameters of nanocubes are always underestimated except for the 5 nm nanocube. To understand the root cause of this difference, we also performed Line Profile Analysis (LPA) on both spherical and cubic ideal nanocrystals. Unlike Rietveld refinement which imposes a unique crystal unit cell and assigns relative intensities to all Bragg peaks based on Eq.2, LPA treats all Bragg peaks independently. This makes it possible to obtain better fits and higher accuracy in individual peak profile parameters, such as peak centers and maxima, at the expense of a unique crystallographic unit cell parameter. Therefore, LPA was used to investigate angle-dependent variations of lattice parameters.

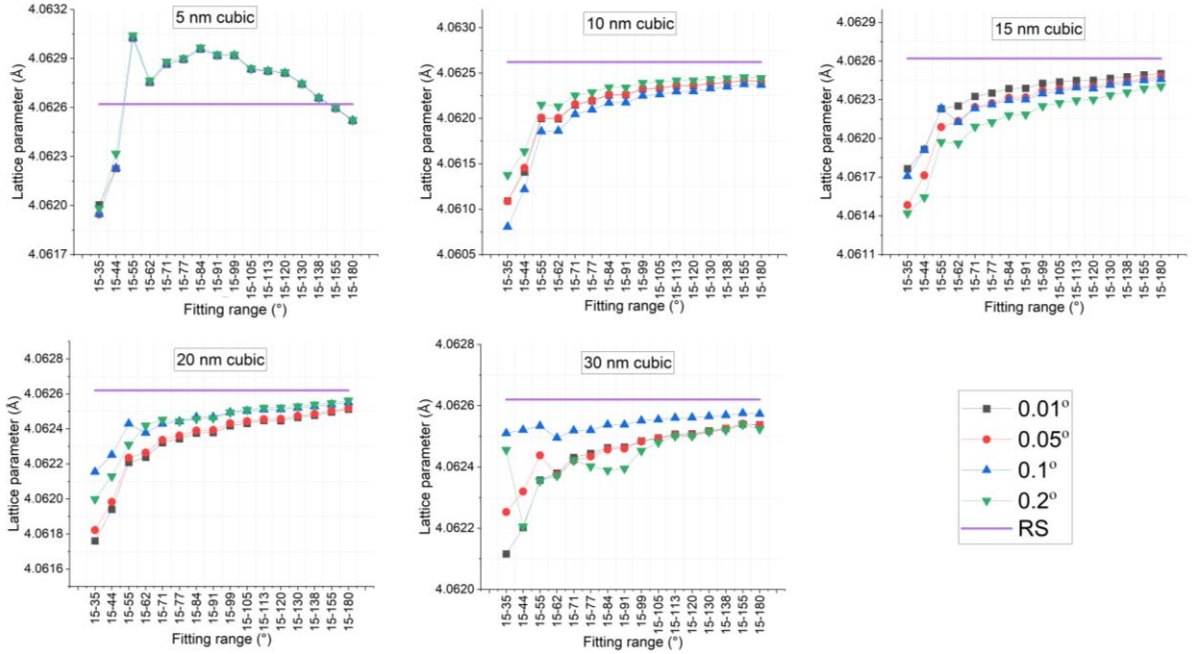

Figure 6: The variations of lattice parameter using different angular ranges for cubic ideal nanoparticles.

For all our datasets, LPA was implemented by fitting a separate Gaussian profile function to each Bragg peak and refining the sum of all functions against the computed diffraction data with a least square error minimization scheme. The Gaussian peak profiles were justified since our hypothetical samples did not include any microstructural defects affecting the Bragg peak profiles(24), there was no additional peak profile modifications due to the incoming X-ray beam(25) and the mixing parameters (LGmix) we obtained from Rietveld refinement of the diffraction datasets were smaller than 0.5 indicating that our Bragg peaks resembled more to Gaussian rather than Lorentzian profiles. For consistency with Rietveld refinement, no background was subtracted during fitting. Once all peaks converged, their peak centers were collected and converted to the corresponding lattice parameters by Bragg's law and the interplanar spacing relation valid for cubic crystals, $2d_{hkl}Sin\theta_{hkl} = \lambda$ and $d_{hkl} = \frac{a}{\sqrt{h^2+k^2+l^2}}$. Table 3 summarizes the results of this analysis.

Table 3: Lattice parameters obtained by LPA from the diffraction data of ideal crystalline gold nanospheres and nanocubes (dθ=0.01°).

Peaks	5nm sphere ideal (Å)	5nm cubic ideal (Å)	10nm sphere ideal (Å)	10nm cubic ideal (Å)	15nm sphere ideal (Å)	15nm cubic ideal (Å)	20nm sphere ideal (Å)	20nm cubic ideal (Å)	30nm sphere ideal (Å)	30nm cubic ideal (Å)
1 1 1	4.065797	4.065816	4.063491	4.06339	4.062977	4.06298	4.062826	4.062824	4.062701	4.062702
2 0 0	4.066810	4.061720	4.063396	4.062009	4.062923	4.06222	4.062791	4.062331	4.062686	4.062444
2 2 0	4.064353	4.062726	4.063052	4.06253	4.062791	4.062535	4.062714	4.06255	4.062651	4.062568
3 1 1	4.064332	4.063807	4.062917	4.062879	4.062745	4.062747	4.062689	4.062696	4.062641	4.062652
2 2 2	4.063548	4.066964	4.063564	4.063265	4.062833	4.062856	4.062717	4.062739	4.062644	4.062655
4 0 0	4.063111	4.061855	4.062848	4.062414	4.062708	4.062482	4.062662	4.062515	4.062625	4.062552
3 3 1	4.064982	4.063775	4.062565	4.062708	4.062653	4.062687	4.062644	4.062669	4.062624	4.062641
4 2 0	4.062124	4.062939	4.063127	4.062671	4.062744	4.062583	4.062672	4.062581	4.062628	4.062593
4 2 2	4.063207	4.063064	4.062778	4.06268	4.062675	4.062629	4.062645	4.062619	4.062621	4.062618
3 3 3	4.063355	4.063201	4.062753	4.062724	4.06266	4.062667	4.062635	4.062646	4.062615	4.062633
4 4 0	4.061254	4.061619	4.062625	4.062453	4.062625	4.06254	4.062616	4.062558	4.062608	4.062577
5 3 1	4.062840	4.062840	4.062639	4.062556	4.062574	4.062622	4.0626	4.062628	4.062605	4.062625
4 4 2	4.062210	4.062210	4.062912	4.063026	4.062787	4.062693	4.062667	4.062639	4.062616	4.062623
6 2 0	4.062621	4.062237	4.062624	4.062547	4.062614	4.062597	4.062609	4.062613	4.062603	4.06262
5 3 3	4.063275	4.063308	4.062683	4.062393	4.062492	4.062519	4.062564	4.062575	4.062594	4.062606
6 2 2	4.062301	4.062300	4.062579	4.062847	4.062717	4.06266	4.06264	4.062607	4.062608	4.062604
4 4 4	4.061247	4.061811	4.062394	4.062607	4.062558	4.062629	4.062583	4.06264	4.062598	4.062659
5 5 1	4.062514	4.063091	4.062683	4.062508	4.06252	4.062551	4.06256	4.062584	4.062589	4.062608
6 4 0	4.062989	4.062069	4.062379	4.062824	4.06284	4.062646	4.062684	4.062579	4.062609	4.062581
6 4 2	4.061839	4.062021	4.062451	4.062553	4.062546	4.062596	4.06257	4.062603	4.062587	4.062602
5 5 3	4.062105	4.062489	4.062444	4.062548	4.062531	4.062584	4.062558	4.062597	4.062581	4.062609
Mean	4.063182	4.062946	4.062805	4.062673	4.062691	4.062620	4.062649	4.062609	4.062621	4.06261
Std	0.001419	0.001325	0.000348	0.000303	0.000135	0.000146	7.19747E-05	9.32339E-05	3.05669E-05	5.08219E-05
%dev	-0.01432	-0.00851	-0.00504	-0.0018	-0.00224	-0.0005	-0.00123	-0.00023	-0.00051	-0.0002

The first column of Table 3 shows the Miller indices of the Bragg peaks, and the remaining columns report the corresponding lattice parameters. As seen, the lattice parameters of cubic and spherical nanocrystals vary from one reflection to another, in general they decrease as the Miller indices increase but there is no clear trend as to which particle shape has a larger or smaller lattice parameter. However, comparing lattice parameters of nanospheres and nanocubes of the same size, we see that for the first 4 Bragg peaks having the highest intensities (see Figure 2), the lattice parameter of the spherical nanocrystal is always overpredicted whereas that of the cubic nanoparticle is underpredicted from the second and the third Bragg reflections. Since Rietveld-refined lattice parameters are a complicated average biased towards lattice parameters from higher intensity Bragg peaks, including these two Bragg peaks in the refinement range may cause the overall refined lattice parameter to be underpredicted for the cubic particle. An exception seems to be the 5 nm nanocube, however unlike larger nanocubes, here the third Bragg peak deviates positively from the true lattice parameter shifting the Rietveld-refined lattice parameter upwards from 4.0626 Å. This concept was mentioned in our previous study(7) as well: while insufficient number of scatters causes positive or negative shifts in the diffraction peak centers from predictions of the Bragg's law, the sign and amount of shift depends also on the X-ray wavelength selected and the shape of the nanocrystal. Hence, it is not surprising to see difference between the Rietveld-refined lattice parameters of spherical and cubic crystallites as well as how closely they agree with the true lattice parameters of the system. Finally, the last three rows of Table 3 report Mean, std and %dev which are the average lattice parameter, standard deviation and percent deviation of the mean lattice parameters from the true value, i.e., 4.0626 Å, respectively. Looking at the arithmetic mean and standard deviations of LPA-based values for each nanocrystal, we notice that although both the lattice parameters of spherical and cubic nanocrystals are greater than their true value, the lattice parameter of the spherical nanocrystal has higher deviations from the true lattice parameter compared to the cubic nanocrystal with the same size. This conclusion also holds for the deviations of Rietveld-refined lattice parameters from their true values seen in Figures 3 and 6 and it can again be explained by the greater number of atoms contained in a cubic nanocrystal compared to a spherical nanocrystal of the same size: the higher the number of scatters, the better the convergence of the refined lattice parameter to its true value.

4.2. Accuracy of Refined Crystal Sizes

The second crystallographic parameter we discuss is the average crystal sizes from Rietveld refinement of diffraction data. Figure 7 demonstrates the variation of refined crystal size for ideal crystalline gold nanospheres for different fitting ranges. Note that here the particle size and crystal size refer to the same physical quantity which is the linear dimension of one nanoparticle since all nanocrystal models were built as single crystalline particles. As seen in all nanoparticles studied, Rietveld-refined average particle sizes are less than the true average diameter (D_{RS}) of the nanocrystals shown by horizontal lines (also see Table 1). Unlike the case for lattice parameters, the refined sizes are stable with some random fluctuation for all fitting ranges selected. This is expected since the studied particles had isotropic shapes which did not depend on the crystallographic direction. Looking at the step sizes of the diffraction data, no generalizable trend between the step size and refined particle size is detected. This indicates that if there is no local variation in the lattice parameters of the nanocrystals which was the case for our ideal crystalline nanopowders, the angular dependence of the peak broadening, β(2θ), is accurately predicted by the Scherrer relation(21) which predicts a variation proportional to 1/cosθ.

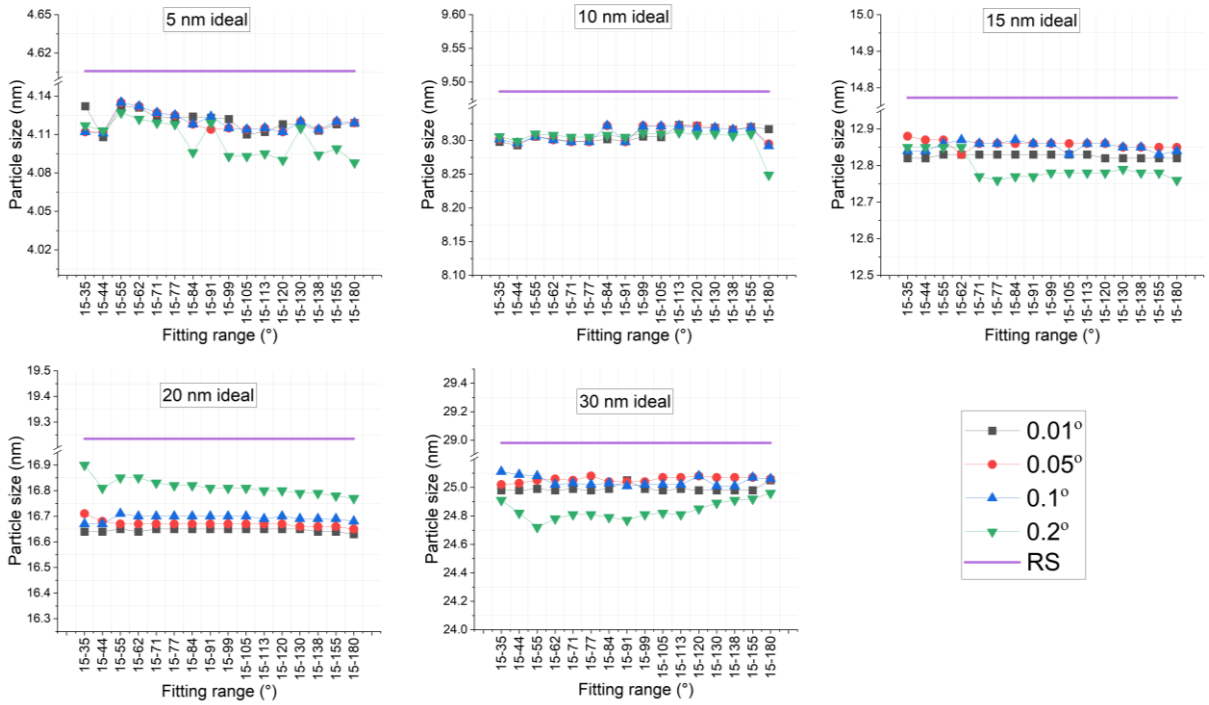

Figure 7: The variations of particle size using different angular ranges for ideal crystalline gold nanospheres. Axis breaks are used to enhance the readability of particle sizes.

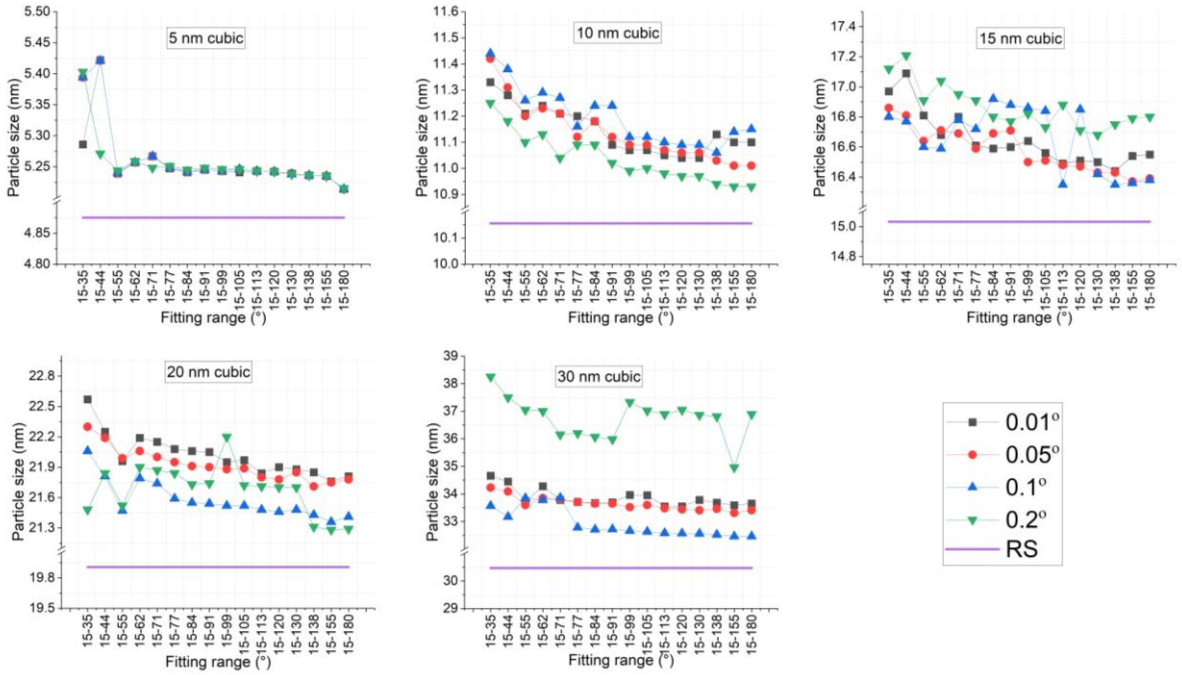

Figure 8: The variations of particle size using different angular ranges for ideal crystalline gold nanocubes.

Repeating this analysis on the diffraction profiles of ideal nanocubes resulted in the data presented in Figure 8. In contrast to spherical nanocrystals, here all Rietveld-refined particle sizes are larger than the true linear dimensions (t_{rs}). Similar to spherical nanocrystals, a smaller step size does not necessarily improve the accuracy of the refined sizes except for the 30 nm nanocrystal: for this particle the peak broadening due to limited crystal size is minimum and Bragg peaks are sharper than smaller cubic crystals. Hence a larger step size causes enhanced inaccuracies in the peak broadening estimations. In addition, a cubic crystal contains a larger number of atoms than a spherical crystal of the same size as seen in Table 1. Therefore, the intensities of cubic crystals are much sharper than those of spherical crystals of the same shape as shown in Figure 1. This enlarged peak sharpness causes further challenges in peak broadening estimation in diffraction data of cubic nanocrystals computed with large step sizes. Overall, these factors explain the worst performance of the particle size refinement with large step size in the 30 nm cubic nanocrystals. In other nanocrystal sizes, the refined sizes seem to fluctuate randomly around a mean and they are almost independent of the step size for the smallest nanocrystal with the broadest Bragg peaks. However, unlike ideal crystalline gold nanospheres, a slight decay in the refined sizes with increasing refinement range is detected. We believe this may be a consequence of the anisotropy in the linear dimensions of the nanocubes which causes slightly different peak broadening terms for different family of hkl reflections and is neglected in modeling the peak-breadth variations over the angular range by GSAS II.

A second factor that may explain the increased fluctuations of refined sizes of nanocubes compared to nanospheres is the difference in the fitting qualities. Note that unlike lattice parameters which only depend on the center of the Bragg peaks, crystallite sizes which depend on the peak breadth are much more dependent on how well the Bragg peak shapes are modeled by the selected analytical functions. One may see in Figure 2 that a mixture of Gaussian-Lorentzian peak profile function captures the main features of Bragg peaks from spherical nanocrystals well, but it is not as successful for Bragg peaks from cubic nanocrystals. This phenomenon is especially visible in the first Bragg peak of the 5 nm nanocube where relatively high residuals are visible around the tail of the peak. It shows that, even though the Rietveld refinements from both cubic and spherical nanocrystals converged successfully, they did not approximate the measured diffraction data equally well as confirmed by the higher normalized weighted residuals of cubic nanocrystals shown in Figure 9. We emphasize that the weighted residuals alone are not the best criterion to judge the goodness of the fitted model; however, visual inspection also confirms that the assumed peak profiles resulted in poorer fit quality for cubic crystals.

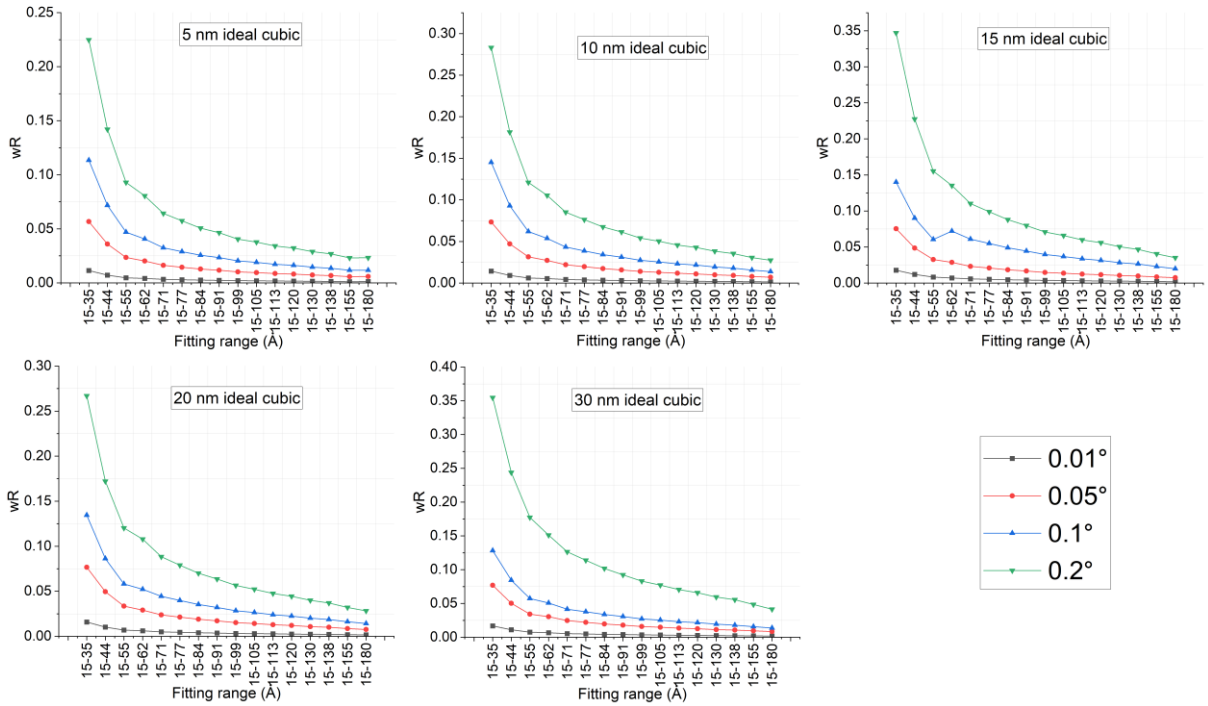

Figure 9: The weighted residuals (wR) normalized by the number of measurement points from Rietveld refinement of diffraction data computed with different step sizes of ideal cubic crystalline gold nanospheres.

Finally, the fact that refined particle sizes from cubic nanocrystals are overestimated while they are underestimated from spherical nanocrystals intimates that the prefactor multiplying the inverse of the peak breadth to the crystal size in the Scherrer equation, i.e. $D_{hkl} = \frac{C\lambda}{\beta_{hkl}\cos\theta_{hkl}}$, may have an effect in the size errors. To confirm this, we checked the value of the shape constant C assumed in GSAS II and found it was equal to one. In the literature, it is a common practice to set the value of C close to unity(26-28). However, this prefactor has been a source of confusion in the past literature of powder diffraction analysis since the concepts such as peak breadth, integral breadth and the meaning of crystal size were not rigorously explained or interpreted. One publication that addressed this issue was written by Patterson(29) where Scherrer constants for spherical crystals were derived by two approaches, one exact and one approximate, for two different breadth definitions: full width at half maximum and integral breadth. According to this study, different definitions of the peak breadth resulted in different values for the prefactor in the Scherrer equation. Recently we worked out the derivation of these Scherrer constants and tested their validity on computer-generated diffraction profiles of spherical crystals formulated by Patterson function(30). We found that the full-width-at-half-maximum based Scherrer constant for cubes were less than 1 (ranging from 0.886 to 0.907 depending on the hkl reflection(31)) while those of spheres were greater than 1 (1.16 for all reflections). This difference in the Scherrer constants of cubic and spherical nanocrystals therefore explains why Rietveld-refined crystal sizes are ≈10% greater than the true sizes for cubic nanocrystals and ≈12% less than those of spherical nanocrystals.

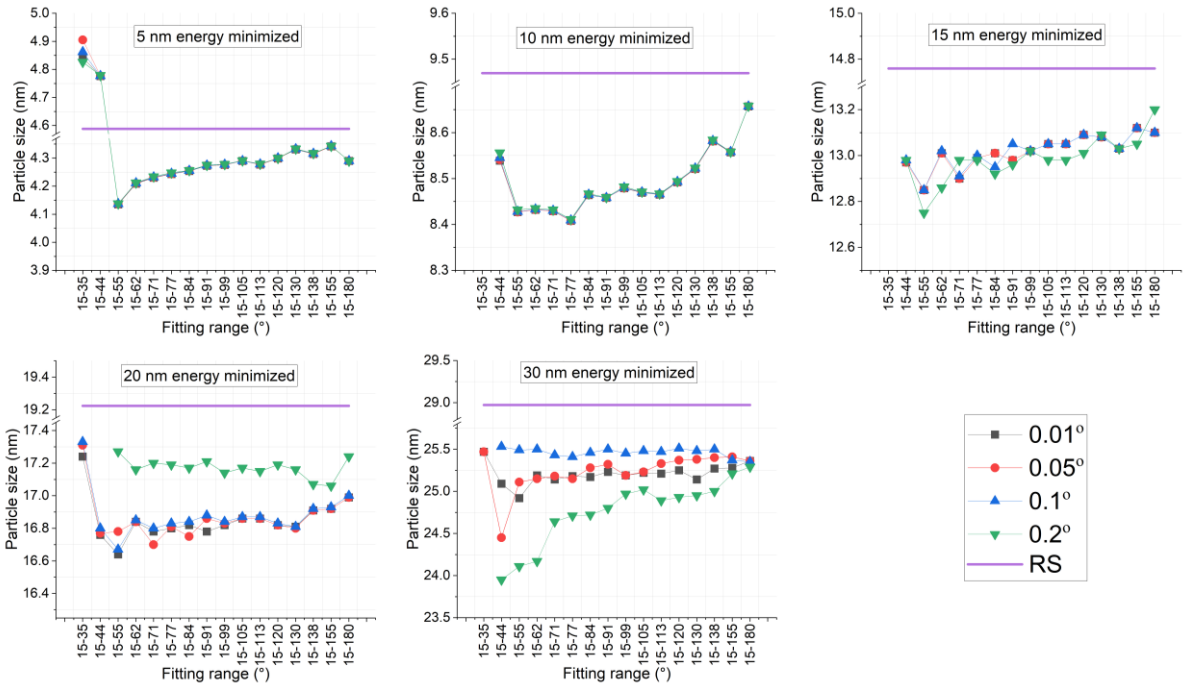

Figure 10: The variations of refined particle size using different angular ranges for energy-minimized nanospheres.

Switching our attention to the crystal sizes refined from diffraction profiles of energy-minimized gold nanospheres, we see similar trends in Figure 10 with ideal crystalline nanospheres shown in Figure 7. For all nanocrystals, the refined particle sizes are smaller than their true mean diameters shown by horizontal lines (see Table 1). For the smallest nanospheres, the angular step size has negligible effect on the refined crystal sizes irrespective of the selected fitting range. Unlike ideal crystalline nanospheres, however, the fitting range has a greater influence on the refined crystal sizes of energy-minimized nanospheres since for these particles the atoms were allowed to relax and were slightly displaced towards particle center compared to their ideal lattice points. This caused slight distortions in particle shape and variations of diameters along different crystallographic directions. Because each Bragg peak yields the crystal size along a different direction, variations of refined size over the fitting range are justified due to the atomic displacements within the surface layer. Comparing average sizes of gold nanospheres before and after the energy minimization process by real space calculations (see Table 1), we find that the true mean diameters decreased slightly with the highest diameter reduction occurring in the smallest nanocrystal due to significant surface relaxation process. Interestingly, refined crystal sizes from energy-minimized nanospheres turned out to be slightly higher than those of ideal crystalline counterparts. Although it is hard to identify the reason behind these slightly larger crystal sizes - since the refinement scheme applied on the diffraction data of ideal crystalline and energy minimized gold nanospheres were different- a chain of events during the refinement of diffraction data seems to be the cause: the Bragg peaks computed from energy-minimized models of nanospheres were slightly broader than those of ideal crystalline nanospheres as seen in Figure 1. However, the refinement scheme applied on the diffraction data of energy-minimized nanospheres included both microstrain and crystal size refinements unlike ideal crystalline nanospheres where only crystal size contributed to peak breadth. Hence a portion of the enhanced peak broadening of energy-minimized nanospheres was attributed to the apparent microstrains. Consequently, not all but a portion of the peak broadening was treated as resulting from limited crystal size which possibly led to slightly larger crystal sizes in energy minimized nanospheres. In conclusion, the refined crystal sizes from energy-minimized nanospheres were approximately 12% less than their true mean diameters.

4.3. Variation of the Refined Microstrains

For classical crystalline powders with particle sizes above 100 nm, a single unit cell is enough to represent the full atomic configuration inside individual particles since for such particles the surface to volume ratio is negligibly small. For nanocrystalline powders, however, surface atoms make up a significantly large proportion of all atoms in the particle and therefore the atomic configuration cannot be represented by a unique rule even at 0 K temperature at which all atoms are frozen at their designated positions(7). This results from the undercoordinated surface atoms in nanocrystals which get displaced towards the particle center to minimize the overall energy of the particle. Once the minimum energy configuration is established, a single unit cell no longer represents the positioning of atoms in the nanocrystal; a significant variation in interplanar spacings between atomic planes from the particle core to the particle surface occurs. In this section we analyze how these static atomic displacements of surface atoms show as broadening of Bragg peaks, therefore

treated as apparent microstrains in Rietveld refinement of the diffraction data, and how refined microstrains vary with refinement range and step size of the diffraction data.

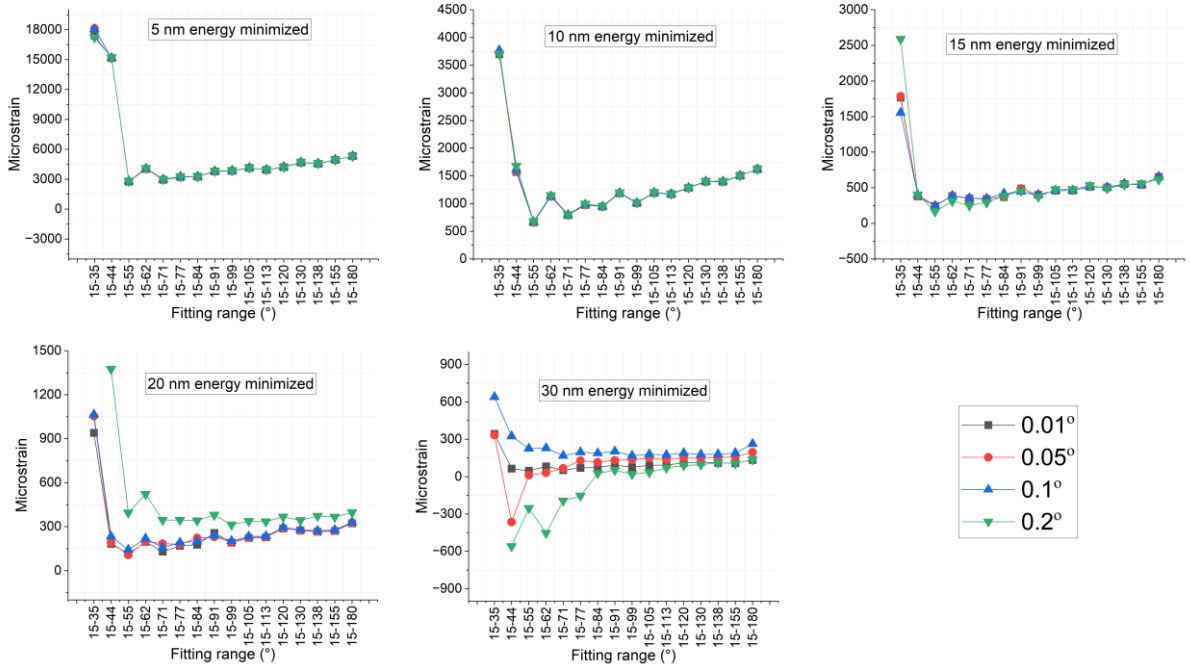

Figure 11: The variations of apparent microstrain from Rietveld refinement using different angular ranges for energy-minimized gold nanospheres.

Figure 11 presents the refined (apparent) microstrains from diffraction data of energy minimized gold nanospheres. These are isotropic microstrains which are assumed to be independent of the crystallographic direction, so a single value is computed and treated as a measure of the average microstrain in the powder. Unlike previous sections, these graphs do not include a true value, since an appropriate real space computation compatible with the microstrain definition in X-ray diffraction analysis is not available in the literature(12). We see that for all nanocrystals, the refined microstrains are maximized for limited refinement range and decay down to stable values as the refinement range increases and includes more Bragg peaks. Among different nanocrystals, the highest values at limited refinement range as well as the ultimate values at extended refinement range are observed for 5 nm nanocrystals for all step sizes. This is because the atomic configuration in the smallest nanocrystal suffers from the greatest amount of surface reconstruction and interplanar spacing variations in the nanocrystal surface contribute to significant peak broadening. In all nanocrystals, the high initial refined microstrains decay and stabilize beyond 55°, which corresponds to the angular range containing the first five Bragg peaks (see Figure 1). The fact that refined microstrains stabilize around the same refinement range for all nanocrystal sizes indicates that refined microstructural parameters are predominantly determined by the Bragg peaks with the highest intensity, which are the first four Bragg peaks in gold crystals. Among different particle sizes, the amount of over- or under-prediction from the ultimate refined microstrains is also much higher for smaller nanocrystals than larger ones. This probably stems from the greater effect of surface atoms and their large atomic displacements on the diffraction profiles which cause their refinement to be more challenging and harder to converge to a unique crystallographic solution especially when the refinement range is limited. Normalized weighted residuals shown in Figure 12 also support this conclusion where the highest residuals are observed from the smallest nanospheres with the largest step sizes of diffraction data. Finally, similar to the refined lattice parameters and average crystal sizes, the step size has an increasing effect on the refined microstrains for larger nanocrystals than smaller ones. This is because estimating the broadening of sharper peaks is more challenging and prone to errors which causes variations in the refined microstrains of larger nanocrystals. An improper selection of step size while measuring diffraction data may result in even negative and unphysical refined microstrains such as those observed in 30 nm gold nanospheres at $d\theta=0.2^{\circ}$.

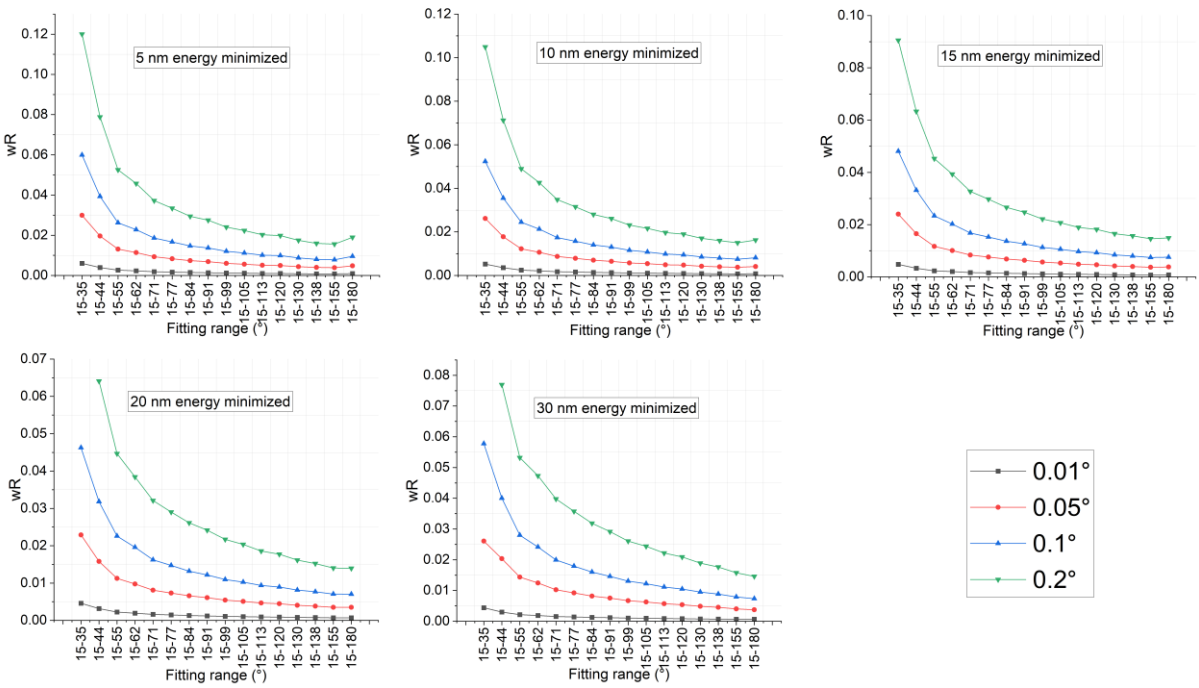

Figure 12: The weighted residuals (wR) normalized by the number of measurement points from Rietveld refinement of diffraction data computed with different step sizes of energy minimized crystalline gold nanospheres.

These results demonstrate that apparent microstrains refined from diffraction data of nanocrystalline powders are never zero even at 0 K. As the crystal size increases to 30 nm, the extended-range refined microstrains approach a value of ≈ 200 which can be considered almost zero since a microstrain value of 1000 is considered typical for bulk crystalline powders measured at room temperature(32).

5. CONCLUSIONS

In this work, we presented a systematic analysis of Rietveld refinement performed on analytical X-ray diffraction profiles from small gold nanocrystals ranging from 5 to 30 nm in size. The variation of refined average lattice parameters, average crystallite sizes and apparent microstrains with respect to 1) step size of the diffraction data, 2) crystal shape and 3) refinement range was investigated. Three model systems were studied for this purpose: ideal crystalline nanospheres, ideal crystalline nanocubes and energy-minimized nanospheres by Molecular Dynamics simulations. Our analysis showed the following:

Lattice parameters obtained from Rietveld refinement improved with increasing refinement range for all nanocrystal systems. Limited refinement range caused overestimations of lattice parameters in spherical ideal and energy-minimized nanocrystals whereas it caused underestimations in the case of cubic nanocrystals. The opposite trend in spherical and cubic nanocrystals was explained to stem from opposite shifts of refined Bragg peak centers for some of the most intense Bragg peaks in cubic gold nanocrystals which were the first four peaks within the diffraction spectra. Comparing energy-minimized and ideal crystalline nanospheres, the former system resulted in larger deviations from the true lattice parameters than the latter which indicated that static atom displacements in small nanocrystals affected the accuracy of refined lattice parameters from their diffraction data. The step size of the diffraction data had negligible effect on the refined lattice parameters of the smallest nanocrystals whereas it became more important for larger nanocrystals which had much sharper Bragg peaks. However, no clear relation was detected between smaller step size in the diffraction data and higher accuracy in the Rietveld-refined lattice parameters as long as the step size was not too wide. For a step size of 0.2°, large fluctuations were detected, and these were attributed to increased fitting errors in Rietveld refinement resulting from the number of measurement points over the Bragg peak range being too few. Our results were consistent with past work from the literature(33).

2) Crystallite sizes obtained from Rietveld refinement were stable over the refinement range for ideal crystalline gold nanospheres. This indicated that the Scherrer-predicted 1/cosθ variation of size-related peak broadening accurately represented the variation of breadth over different reflections. This was not the case for ideal crystalline nanocubes where much higher fluctuations than those in ideal crystalline nanospheres were present over the refinement range. These fluctuations were attributed to the anisotropic linear dimensions of cubic nanocrystals and higher residuals of the refined profiles. The refined crystal sizes for ideal spheres were ≈10% lower than the true mean diameters whereas they were ≈12% higher than the thicknesses of ideal cubes. Incompatible Scherrer shape constant was found to cause this difference between the Rietveld-refined and true

dimensions of spherical and cubic nanoparticles. Smaller step size of the diffraction data helped better modeling of the peak profile, but its effect was negligible for the smallest nanocrystals. Although larger nanocrystals having much sharper Bragg peaks required much smaller step size for accurate profile modelling, we could not correlate smaller step size with higher accuracy in the refined crystallite sizes. Finally, for energy-minimized gold nanospheres, Rietveld-refined average diameters were more dependent on the refinement range. This was because peak broadening was contributed by two factors in these systems: static atomic displacements acting like apparent strains in the particle and limited crystal size. Modelling peak breadth and separating different broadening contributions to each Bragg peak necessitated several Bragg peaks increasing the refinement range.

3) Rietveld refinement of static displacements in the form of apparent microstrains for energy-minimized gold nanospheres were strongly dependent on the refinement range. Short refinement range including only 2-3 Bragg peaks resulted in large apparent microstrains which decreased with increasing refinement range. Refinement range was especially critical for the smallest nanocrystal which was affected by the largest amount of surface reconstruction and associated static atom displacements. Unfortunately, we did not have analytical formulations to predict the true values of static displacements hence we could not infer the accuracy of the values obtained from Rietveld refinement in this case. However, for 30 nm nanocrystals, the refined microstrains approached a value which was 20% of what was considered typical for unstressed regular crystalline powders measured at room temperature. For all nanocrystal sizes, a refinement range beyond 55° was found sufficient to obtain stabilized values for refined microstrains.

These results show that for gold nanocrystals having an average size of 30 nm and above, the diffraction data must be collected with a step size less than ≈0.2° to avoid large fluctuations in the Rietveld-refined crystallographic parameters. This step size is consistent with past work as well(33). For smaller nanocrystals, the largest step size resulting in stable crystallographic parameters from Rietveld refinement is expected to be larger than 0.2°. For highest accuracy in refined lattice parameters and crystal sizes, selecting as wide of a refinement range as possible is suggested. Although this sounds somewhat contrary to the claims by Uvarov reporting no appreciable difference in refined lattice parameters and crystal sizes (23) with increased refinement range, the minimum refinement range selected in that work was 60°, the smallest particle size of samples measured was 10 nm, most of the studied samples were of mixed phase and the Rietveld analysis was performed on measured diffraction data necessitating several more parameters to be simultaneously refined, including background scattering. Therefore, it is unclear whether some of the nanoscale features we observed in our analytical diffraction data were observable in their measurements. Finally, nanocrystal shape has a significant effect on the performance of Rietveld refinement of nanocrystalline powders. However, these effects are expected to be less severe in the analysis of diffraction data measured from realistic powders consisting of a distribution of particle sizes and shape. In that case, the results would be more biased towards the larger particle and its shape.

6. ACKNOWLEDGMENTS

We thank to Mr. Merdan Batyrow for performing Molecular Dynamics simulations to generate energy-minimized models of gold nanospheres and reviewing our manuscript. This research was funded by the Turkish Scientific and Technological Research Council (TUBİTAK) under the BİDEB 2232 program (Project no: 118C268).

7. SUPPORTING INFORMATION

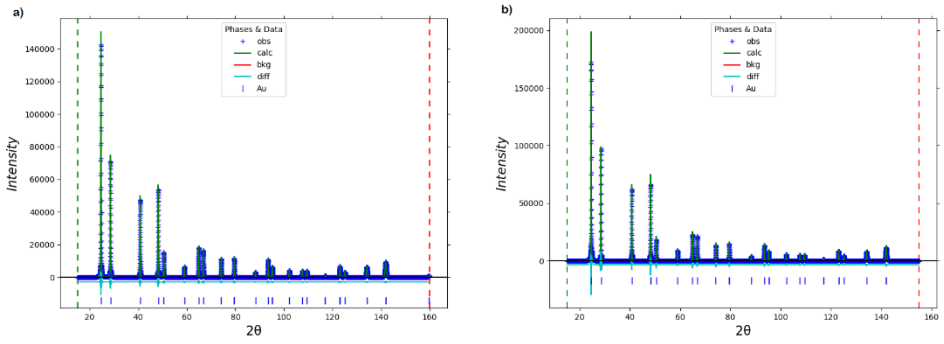

Figure S1: A successful Rietveld refinement of the diffraction data from a 30 nm ideal crystalline nanosphere (left) and a 30 nm ideal crystalline nanocube. The blue tick marks show the expected positions of the Bragg peaks predicted by Bragg's law.

REFERENCES

1. Rietveld HM. A profile refinement method for nuclear and magnetic structures. J Appl Crystallogr [Internet]. 1969 Jun 2;2(2):65–71. Available from: <URL>.

2. Cullity BD. Elements of X-ray Diffraction. Addison-Wesley Publishing Company; 1978.

3. Ingham B. X-ray scattering characterisation of nanoparticles. Crystallogr Rev [Internet]. 2015 Oct 2;21(4):229–303. Available from: <URL>.

4. Öztürk H, Yan H, Hill JP, Noyan IC. Sampling statistics of diffraction from nanoparticle powder aggregates. J Appl Crystallogr [Internet]. 2014 Jun 1;47(3):1016–25. Available from: <URL>.

5. Öztürk H, Yan H, Hill JP, Noyan IC. Correlating sampling and intensity statistics in nanoparticle diffraction experiments. J Appl Crystallogr [Internet]. 2015 Aug 1;48(4):1212–27. Available from: <URL>.

6. Fewster PF. A new theory for X-ray diffraction. Acta Crystallogr Sect A Found Adv [Internet]. 2014 May 1;70(3):257–82. Available from: <URL>.

7. Xiong S, Öztürk H, Lee SY, Mooney PM, Noyan IC. The nanodiffraction problem. J Appl Crystallogr [Internet]. 2018 Aug 1;51(4):1102–15. Available from: <URL>.

8. Warren BE. X-ray Diffraction. New York: Dover Publications; 1990.

9. Larson AC, Von Dreele RB. GSAS General Structure Analysis System [Internet]. Available from: <URL>.

10. McCusker LB, Von Dreele RB, Cox DE, Louër D, Scardi P. Rietveld refinement guidelines. J Appl Crystallogr [Internet]. 1999 Feb 1;32(1):36–50. Available from: https://scripts.iucr.org/cgi-bin/paper?S0021889898009856

11. Young RA. The Rietveld Method. Powder Diffr [Internet]. 1993 Dec 10;8(4):252–4. Available from: <URL>.

12. Xiong S, Lee SY, Noyan IC. Average and local strain fields in nanocrystals. J Appl Crystallogr [Internet]. 2019 Apr 1;52(2):262–73. Available from: <URL>.

13. Baloochiyan A, Batyrow M, Öztürk H. Accuracy Limits of Pair Distribution Function Analysis in Structural Characterization of Nanocrystalline Powders by X-ray Diffraction. J Turkish Chem Soc Sect A Chem [Internet]. 2022 May 31;9(2):527–44. Available from: <URL>.

14. Batyrow M, Eruçar İ, Öztürk H. Size dependent change of mean square displacement in gold nanocrystals: A molecular dynamics simulation. Concurr Comput Pract Exp [Internet]. 2023 Nov 12;35(24):e7566. Available from: <URL>.

15. Debye P. Zerstreuung von Röntgenstrahlen. Ann Phys [Internet]. 1915 Jan 14;351(6):809–23. Available from: <URL>.

16. Warren BE. X-Ray Diffraction. Dover Publications; 2012.

17. Alexander L, Klug HP, Kummer E. Statistical Factors Affecting the Intensity of X-Rays Diffracted by Crystalline Powders. J Appl Phys [Internet]. 1948 Aug 1;19(8):742–53. Available from: <URL>.

18. Debyer. Debyer documentation [Internet]. [cited 2024 Jun 10]. Available from: <URL>.

19. Toby BH, Von Dreele RB. GSAS-II : the genesis of a modern open-source all purpose crystallography software package. J Appl Crystallogr [Internet]. 2013 Apr 1;46(2):544–9. Available from: <URL>.

20. Williamson G., Hall W. X-ray line broadening from filed aluminium and wolfram. Acta Metall [Internet]. 1953 Jan;1(1):22–31. Available from: <URL>.

21. Scherrer P. Bestimmung der inneren Struktur und der Größe von Kolloidteilchen mittels Röntgenstrahlen. In: Kolloidchemie Ein Lehrbuch [Internet]. Berlin, Heidelberg: Springer Berlin Heidelberg; 1912. p. 387–409. Available from: <URL>.

22. Stephens PW. Phenomenological model of anisotropic peak broadening in powder diffraction. J Appl Crystallogr [Internet]. 1999 Apr 1;32(2):281–9. Available from: <URL>.

23. Uvarov V. The influence of X-ray diffraction pattern angular range on Rietveld refinement results used for quantitative analysis, crystallite size calculation and unit-cell parameter refinement. J Appl Crystallogr [Internet]. 2019 Apr 1;52(2):252–61. Available from: <URL>.

24. Ungár T. Microstructural parameters from X-ray diffraction peak broadening. Scr Mater [Internet]. 2004 Oct;51(8):777–81. Available from: <URL>.

25. Rebuffi L, Sánchez del Río M, Busetto E, Scardi P. Understanding the instrumental profile of synchrotron radiation X-ray powder diffraction beamlines. J Synchrotron Radiat [Internet]. 2017 May 1;24(3):622–35. Available from: <URL>.

26. Yager KG, Majewski PW. Metrics of graininess: robust quantification of grain count from the non-uniformity of scattering rings. J Appl Crystallogr [Internet]. 2014 Dec 1;47(6):1855–65. Available from: <URL>.

27. Herklotz M, Scheiba F, Hinterstein M, Nikolowski K, Knapp M, Dippel AC, et al. Advances in in situ powder diffraction of battery materials: a case study of the new beamline P02.1 at DESY, Hamburg. J Appl Crystallogr [Internet]. 2013 Aug 1;46(4):1117–27. Available from: <URL>.

28. Smilgies DM. Scherrer grain-size analysis adapted to grazing-incidence scattering with area detectors. J Appl Crystallogr [Internet]. 2009 Dec 1;42(6):1030–4. Available from: <URL>.

29. Patterson AL. The Scherrer Formula for X-Ray Particle Size Determination. Phys Rev [Internet]. 1939 Nov 15;56(10):978–82. Available from: <URL>.

30. Noyan İC, Öztürk H. Lower uncertainty bounds of diffraction-based nanoparticle sizes. J Appl Crystallogr [Internet]. 2022 Jun 1;55(3):455–70. Available from: <URL>.